

SlotMatch: Distilling Object-Centric Representations for Unsupervised Video Segmentation

Diana-Nicoleta Grigore^{1,*}, Neelu Madan^{2,*}, Andreas Møgelmo², Thomas B. Moeslund²,
Radu Tudor Ionescu^{1,◇}

¹University of Bucharest, Romania, ²Aalborg University, Denmark

*Equal contribution. ◇Corresponding author: raducu.ionescu@gmail.com.

Abstract

Unsupervised video segmentation is a challenging computer vision task, especially due to the lack of supervisory signals coupled with the complexity of visual scenes. To overcome this challenge, state-of-the-art models based on slot attention often have to rely on large and computationally expensive neural architectures. To this end, we propose a simple knowledge distillation framework that effectively transfers object-centric representations to a lightweight student. The proposed framework, called SLOTMATCH, aligns corresponding teacher and student slots via the cosine similarity, requiring no additional distillation objectives or auxiliary supervision. The simplicity of SLOTMATCH is confirmed via theoretical and empirical evidence, both indicating that integrating additional losses is redundant. We conduct experiments on three datasets to compare the state-of-the-art teacher model, SLOTCONTRAST, with our distilled student. The results show that our student based on SLOTMATCH matches and even outperforms its teacher, while using $3.6\times$ less parameters and running up to $2.7\times$ faster. Moreover, our student surpasses all other state-of-the-art unsupervised video segmentation models.

1. Introduction

A fundamental goal in machine perception is developing systems that, as humans, understand complex visual scenes as compositions of distinct objects. This capability, studied in the area of *object-centric representation learning* [3, 12, 24], is a critical step for building agents that can reason about, interact with, and understand their surroundings. Recent advances in self-supervised learning have produced powerful foundational models [4, 14, 26]. When integrated into slot-based attention frameworks [20, 24], these models can discover and segment objects from complex scenes with remarkable fidelity. However, their success is predicated on their scale, as the high computational costs create bottlenecks for deployment. As such, typi-

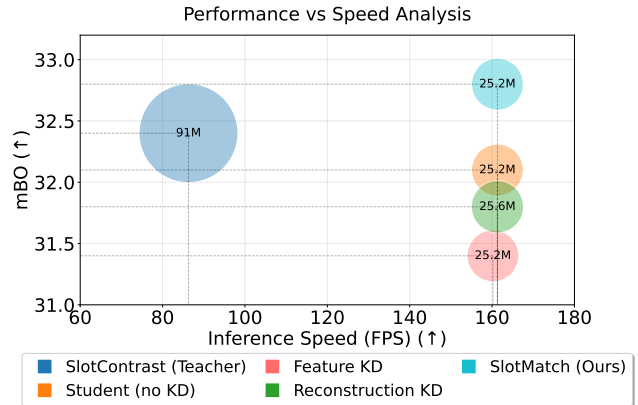


Figure 1. Comparison of SLOTCONTRAST (teacher) versus various student versions (including our SLOTMATCH), showing the trade-off between performance (mean Best Overlap or mBO) vs. inference speed (FPS). Circle area indicates parameter count (in millions). SLOTMATCH (cyan) outperforms its teacher, while being nearly twice as fast on NVIDIA A100. Best viewed in color.

cal self-supervised models are incompatible with resource-constrained environments, where object-centric representations built for video-related tasks would be most valuable.

To overcome this critical trade-off between performance and efficiency, we propose a knowledge distillation strategy tailored for object-centric models. Our method transfers the object discovery capabilities of a large *teacher* model to a lightweight *student*, aiming to create a final model that is not only more suitable for resource-constrained applications, but is also a more effective learner.

Our core contribution is a novel optimization strategy that operates directly on the learned object slots. We frame the primary distillation objective as a direct matching loss, termed SLOTMATCH, where a slot from the student model serves as the “positive” and the corresponding teacher slot provides the fixed (target) “anchor”. This pulls the student’s representation towards the teacher’s proven semantic space. Crucially, the necessary repulsive force is not supplied by explicit negatives in the distillation loss itself. Instead, we

rely on the student’s slot contrastive loss, which is concurrently optimized with the distillation objective. This combination effectively decomposes the learning signal: the distillation loss teaches each slot *what to be*, while the contrastive loss teaches it *not to be* a redundant copy of other slots. We apply a similar principle to the reconstructed features, *i.e.* the student is trained to minimize the mean squared error between its input and output representations, without distilling representations from the teacher. We provide theoretical and empirical evidence confirming that our simple distillation objective is sufficient and effective. More precisely, we show that distilling output features is redundant.

We carry out experiments on three benchmark datasets for unsupervised video segmentation, MOVi-E [9], YTVIS-2021 [33] and DAVIS 2017 [27]. We compare our student based on SLOTMATCH with its state-of-the-art teacher, SLOTCONTRAST [25], as well as other competitive methods from recent literature [1, 19, 20, 30, 31, 34]. The results indicate that our student outperforms state-of-the-art models on all datasets. Furthermore, our student contains $3.6\times$ less parameters and runs up to $2.7\times$ faster than its teacher model, SLOTCONTRAST (see Figure 1 and Table 2).

In summary, our contribution is threefold:

- We introduce SLOTMATCH, a knowledge distillation framework to distill slot attention by minimizing the cosine similarity between corresponding teacher and student slots.
- We provide theoretical evidence indicating that our slot distillation procedure can effectively distill information from the teacher, without requiring additional losses.
- We empirically show that our student based on SLOTMATCH is both effective and efficient, surpassing its teacher in terms of multiple performance metrics, while being $1.9\times$ to $2.7\times$ faster and $3.6\times$ smaller.

2. Related Work

Object-centric representation learning. Unsupervised scene decomposition aims to discover object-based structure in raw perceptual inputs, without supervision. Early methods approached this task via perceptual grouping [10], spatial mixture models [11], or foreground-background separation [32]. Recent approaches focused on *slot attention* [24], which uses iterative attention to bind latent learnable vectors, called *slots*, to individual objects. Since its introduction, the paradigm has been extended to incorporate real-world images [30], auto-regressive decoder with patch-order permutation [18], adaptive slot counts [8], learned-query initialization [17], language-controlled slots [6] and scale-invariant pipelines [2]. While all of these have shown strong results in image-based object discovery, their adaptation to video requires additional mechanisms to ensure temporal consistency.

Object-centric video models. Slot attention was originally extended to video through methods such as SAVi [20] and SAVi++ [7], which introduced cross-frame attention and optical flow to promote temporal coherence. Later, STEVE [31] added sequential latent dynamics for video generation. VideoSAUR [34] and SlotContrast [25] further enhanced the approach with contrastive objectives and stronger backbones, *e.g.* DINOv2 [26]. While effective, these methods typically rely on computationally-intensive encoders, limiting their applicability to real-time or embedded scenarios. Our work addresses this limitation by transferring object-centric knowledge from a high-capacity video model to a lightweight model via distillation.

Knowledge distillation. Knowledge distillation (KD) transfers information from a large “teacher” model to a compact “student” by aligning output distributions [15], intermediate activations [29], or feature Jacobians [5], among others. Most of the existing KD studies are focused on traditional tasks (*e.g.* classification [16], language modeling [13]), with limited application to object-centric learning.

To the best of our knowledge, there are only a few recent papers that explore distillation from scene decomposition [18, 19, 21, 22, 30]. DIOD [19] introduced a self-distillation strategy in video slot attention, where an EMA teacher supervises the student by refining slot masks using optical flow and static cues. DINOSAUR [30] is a framework that distills high-level features from a pre-trained DINOv2 encoder by training a slot-based model to reconstruct them, enabling slot emergence on real-world images. Some works [21] used slot attention to distill object-centric features from an image-based detector to an event-based one via slot-aware cross-modal alignment, while others proposed federated slot learning [22], using a teacher-student decoder setup to distill shared object-centric representations across distributed domains.

Nevertheless, none of the aforementioned studies considers structured slot-based representations. Our approach departs from standard distillation by aligning latent object slots directly, using a simple and effective cosine-based objective in the slot space. To our knowledge, SLOTMATCH is the first method to perform distillation at the level of semantic slot representations in video.

3. Method

We propose SLOTMATCH, a distillation framework designed to transfer temporally-consistent object-centric representations from a large teacher model to a compact student model. Our core insight is to operate directly in the slot space. As such, we introduce a novel similarity-based distillation objective that aligns semantic slot representations between teacher and student models. Unlike standard methods, SLOTMATCH avoids conventional pixel-wise or feature-level distillation, instead relying on a direct seman-

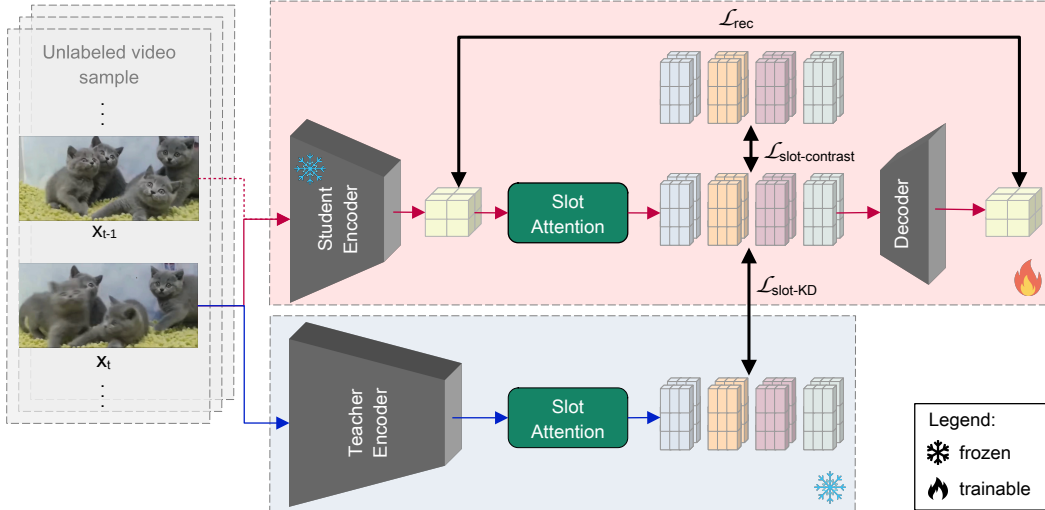


Figure 2. Our SLOTMATCH framework performs knowledge distillation from a large frozen teacher model to a compact trainable student model. Both models process video frames through slot attention mechanisms, with the student learning through three loss components: reconstruction (\mathcal{L}_{rec}), temporal consistency ($\mathcal{L}_{slot-contrast}$), and our novel slot matching loss ($\mathcal{L}_{slot-KD}$) that directly aligns corresponding slots between teacher and student models using cosine similarity. Best viewed in color.

tic match between corresponding slots.

Problem setup. Let \mathbf{T} denote a frozen pre-trained teacher model with a high-capacity encoder, and \mathbf{S} denote a lightweight trainable student. Both operate on video frames and produce a fixed number of slot representations per frame, capturing object-centric semantics. Specifically, for a video frame x_t , the teacher and the student produce the slot representations defined below:

$$\mathbf{S}_t^{\mathbf{T}} = \{s_{t,n}^{\mathbf{T}}\}_{n=1}^N \in \mathbb{R}^{N \times d}, \mathbf{S}_t^{\mathbf{S}} = \{s_{t,n}^{\mathbf{S}}\}_{n=1}^N \in \mathbb{R}^{N \times d}, \quad (1)$$

where each slot $s_{t,n} \in \mathbb{R}^d$ encodes information about a distinct object in the scene. We aim to train the student model such that its slots match the semantics of the teacher, preserve temporal consistency, and support scene reconstruction.

SLOTMATCH framework. In Figure 2, we showcase our SLOTMATCH framework, which operates in a dual-model fashion, with the teacher and student models processing identical video inputs in parallel, through a slot-attention-based encoder-decoder architecture inspired by SlotContrast [25]. First, a pre-trained DINOv2 [26] backbone extracts spatial feature maps from each video frame. The teacher employs a higher-capacity encoder (e.g. ViT-B), while the student uses a lighter variant (e.g. ViT-S). Both encoders are frozen, but they contain a shallow trainable MLP that projects encoder features into a joint d -dimensional slot space. For each frame, we initialize a fixed number of N slots and iteratively update them via attention applied to encoded features. Slot attention compresses scene information into object-centric latent vectors. In the final part, the student employs a decoder that reconstructs the original features from slots. This ensures that slots are informative

and can guide unsupervised segmentation. The teacher also uses a similar decoder during its training phase, but we do not employ it in the distillation stage. To avoid clutter, we refrain from depicting the decoder of the teacher in Figure 2.

Training proceeds as formally described in Algorithm 1. For each mini-batch of B videos with T frames each, we extract per-frame slot representations $\mathbf{S}_{b,t}^{\mathbf{T}}$ and $\mathbf{S}_{b,t}^{\mathbf{S}}$ from the teacher and student models (steps 5 and 7), where b is the video index and t is the frame index. In step 8, a decoder reconstructs the input features from the student slots, producing $\hat{\mathbf{F}}_{b,t}^{\mathbf{S}}$. We next compute three loss terms: (i) a reconstruction loss \mathcal{L}_{rec} to ensure that student slots retain sufficient scene-level information (step 9); (ii) a temporal contrastive loss $\mathcal{L}_{slot-contrast}$ to promote both consistency and diversity of slots across adjacent frames (step 10); and (iii) our core distillation objective $\mathcal{L}_{slot-KD}$ to align each student slot with its teacher counterpart via cosine similarity (step 11). These are combined into a weighted loss (step 12) used to update the student parameters via gradient descent (step 13), while the teacher remains frozen during the whole process.

Slot-level distillation. In the teacher-student training phase, the first issue that arises is to find the correspondence between teacher and student slots, since the slots do not follow a precise order. We consider two options to determine the correspondence among teacher and student slots. One option is to perform explicit matching, e.g. via Hungarian assignment, while the other is to implicitly assume slot index correspondence, i.e. the n -th slot of the student corresponds to the n -th slot of the teacher. We ablate slot correspondence strategies in Table 5 and find negligible difference between Hungarian and direct assignment setups. We

Algorithm 1: SLOTMATCH: Slot-Level Knowledge Distillation

Input: $\mathcal{D} = \{\mathbf{X}_1, \dots, \mathbf{X}_M\}$ – training set of M video sequences, each with T frames;
 $\mathbf{T} = \mathbf{T}^{\text{enc+attn+dec}}$ – pre-trained teacher model with frozen weights $\theta_{\mathbf{T}} = \{\theta_{\mathbf{T}}^{\text{enc}}, \theta_{\mathbf{T}}^{\text{attn}}, \theta_{\mathbf{T}}^{\text{dec}}\}$;
 $\mathbf{S} = \mathbf{S}^{\text{enc+attn+dec}}$ – student model with trainable weights $\theta_{\mathbf{S}} = \{\theta_{\mathbf{S}}^{\text{enc}}, \theta_{\mathbf{S}}^{\text{attn}}, \theta_{\mathbf{S}}^{\text{dec}}\}$;
 α – contrastive loss weight, β – slot distillation weight, η – learning rate; τ – temperature parameter;
 N – number of slots per frame; B – mini-batch size.
Output: $\theta_{\mathbf{S}}$ – learned weights of the student model.

```
1 repeat
2   foreach mini-batch  $\mathcal{B} = \{\mathbf{V}^{(b)}\}_{b=1}^B \subset \mathcal{D}$  do
3     foreach video index  $b \in \{1, \dots, B\}$  do
4       foreach frame index  $t \in \{1, \dots, T\}$  do
5          $\mathbf{S}_{b,t}^{\mathbf{T}} \leftarrow \mathbf{T}^{\text{enc+attn}}(\mathbf{x}_t^{(b)}; \theta_{\mathbf{T}}^{\text{enc}}, \theta_{\mathbf{T}}^{\text{attn}})$   $\triangleleft$  obtain teacher slots of shape  $N \times d$ 
6          $\mathbf{F}_{b,t}^{\mathbf{S}} \leftarrow \mathbf{S}^{\text{enc}}(\mathbf{x}_t^{(b)}; \theta_{\mathbf{S}}^{\text{enc}})$   $\triangleleft$  obtain student features
7          $\mathbf{S}_{b,t}^{\mathbf{S}} \leftarrow \mathbf{S}^{\text{attn}}(\mathbf{F}_{b,t}^{\mathbf{S}}; \theta_{\mathbf{S}}^{\text{attn}})$   $\triangleleft$  obtain student slots of shape  $N \times d$ 
8          $\hat{\mathbf{F}}_{b,t}^{\mathbf{S}} \leftarrow \mathbf{S}^{\text{dec}}(\mathbf{S}_{b,t}^{\mathbf{S}}; \theta_{\mathbf{S}}^{\text{dec}})$   $\triangleleft$  obtain decoded reconstruction
9          $\mathcal{L}_{\text{rec}} \leftarrow \frac{1}{B \cdot T} \sum_{b=1}^B \sum_{t=1}^T \|\hat{\mathbf{F}}_{b,t}^{\mathbf{S}} - \mathbf{F}_{b,t}^{\mathbf{S}}\|^2$   $\triangleleft$  feature reconstruction loss (based on MSE)
10         $\mathcal{L}_{\text{slot-contrast}} \leftarrow \frac{1}{B \cdot T \cdot N} \sum_{b=1}^B \sum_{t=1}^{T-1} \sum_{n=1}^N -\log \frac{\exp(\text{sim}(s_{b,t,n}^{\mathbf{S}}, s_{b,t+1,n}^{\mathbf{S}})/\tau)}{\sum_{b',t',n'} \exp(\text{sim}(s_{b,t,n}^{\mathbf{S}}, s_{b',t',n'}^{\mathbf{S}})/\tau)}$   $\triangleleft$  slot-slot contrastive loss
11         $\mathcal{L}_{\text{slot-KD}} \leftarrow \frac{1}{B \cdot T \cdot N} \sum_{b=1}^B \sum_{t=1}^T \sum_{n=1}^N \left(1 - \frac{\langle s_{b,t,n}^{\mathbf{S}}, s_{b,t,n}^{\mathbf{T}} \rangle}{\|s_{b,t,n}^{\mathbf{S}}\| \cdot \|s_{b,t,n}^{\mathbf{T}}\|}\right)$   $\triangleleft$  distillation loss (based on cosine similarity)
12         $\mathcal{L}_{\text{total}} \leftarrow \mathcal{L}_{\text{rec}} + \alpha \cdot \mathcal{L}_{\text{slot-contrast}} + \beta \cdot \mathcal{L}_{\text{slot-KD}}$   $\triangleleft$  compute combined training objective
13         $\theta_{\mathbf{S}} \leftarrow \theta_{\mathbf{S}} - \eta \cdot \nabla_{\theta_{\mathbf{S}}} \mathcal{L}_{\text{total}}$   $\triangleleft$  update the weights of the student model
14 until convergence;
```

thus adopt the simple direct assignment in our framework.

Each model produces N slot representations of dimension d , each of them encoding semantic information about a distinct object in the scene. The teacher model, through its larger encoder, learns robust object representations via its slots, capturing fine-grained semantic details, which we aim to distill into the student through direct slot alignment.

The core contribution of our method is the introduction of a novel cosine-based slot distillation loss $\mathcal{L}_{\text{slot-KD}}$ that aligns each student slot with its teacher counterpart:

$$\mathcal{L}_{\text{slot-KD}} = \frac{1}{B \cdot T \cdot N} \sum_{b=1}^B \sum_{t=1}^T \sum_{n=1}^N \left(1 - \frac{\langle s_{b,t,n}^{\mathbf{S}}, s_{b,t,n}^{\mathbf{T}} \rangle}{\|s_{b,t,n}^{\mathbf{S}}\| \cdot \|s_{b,t,n}^{\mathbf{T}}\|}\right), \quad (2)$$

where B is the mini-batch size, T is the number of frames in a video, and N is the number of slots. This formulation directly distills the object-centric latent space, promoting structured and efficient knowledge transfer. Each slot from the student serves as a “positive” that must align to its corresponding teacher slot through cosine similarity-based optimization. The target teacher slot serves a fixed “anchor”, since the teacher is completely frozen during distillation. Our formulation creates attractive forces that guide the stu-

dent’s representation toward the teacher’s semantic space.

Temporal and reconstruction losses. Following Manasyan et al. [25], we integrate two auxiliary objectives to improve slot quality for the student, namely the slot-slot contrastive loss ($\mathcal{L}_{\text{slot-contrast}}$), and the feature reconstruction loss (\mathcal{L}_{rec}). This decomposition assigns distinct responsibilities to each loss component. Critically, the absence of explicit negative sampling in the distillation loss is compensated by the concurrent optimization of $\mathcal{L}_{\text{slot-contrast}}$, which provides the necessary repulsive forces to maintain slot distinctiveness for the student. While the slot distillation loss enforces semantic alignment between corresponding teacher-student slot pairs, the slot-slot contrastive loss maintains representational diversity among student slots, ensures temporal consistency by attracting slots representing the same object across consecutive frames, while also repelling slots from different objects within the mini-batch. The feature reconstruction loss \mathcal{L}_{rec} ensures that student slots contain sufficient information to reconstruct features given by the student encoder, via its trainable decoder.

Overall training objective. The complete training objec-

tive integrates all three components:

$$\mathcal{L}_{\text{total}} = \mathcal{L}_{\text{rec}} + \alpha \cdot \mathcal{L}_{\text{slot-contrast}} + \beta \cdot \mathcal{L}_{\text{slot-KD}}, \quad (3)$$

where α and β control the relative importance of temporal consistency and knowledge transfer, respectively. The key advantages of our slot-based approach are its simplicity and efficiency. Unlike methods requiring complex assignment algorithms or feature-level matching, our direct correspondence assumption eliminates computational overhead, while maintaining effective knowledge transfer.

Theoretical justification. We conjecture that it is sufficient to employ the loss in Eq. (2) to perform effective knowledge distillation. In other words, we assume that integrating additional losses, *e.g.* distilling the reconstructed features, is not necessary as long as $\mathcal{L}_{\text{slot-KD}}$ is minimized to zero after training. To support our conjecture, which simplifies the distillation framework, we introduce the following theorem:

Theorem 1. *Let $s^{\mathbf{T}} \in \mathbb{R}^d$ be a teacher slot and $s^{\mathbf{S}} \in \mathbb{R}^d$ a student slot, with $\|s^{\mathbf{T}}\| = \|s^{\mathbf{S}}\| = r$, where $r > 0$. Let $f: \mathbb{R}^d \rightarrow \mathbb{R}^m$ be a K_f -Lipschitz neural network that decodes the slots into features. If the slot distillation loss converges to a constant c , *i.e.*:*

$$\mathcal{L}_{\text{slot-KD}}(s^{\mathbf{T}}, s^{\mathbf{S}}) = 1 - \frac{\langle s^{\mathbf{T}}, s^{\mathbf{S}} \rangle}{\|s^{\mathbf{T}}\| \cdot \|s^{\mathbf{S}}\|} = c, \quad (4)$$

then:

$$\mathcal{L}_{\text{rec-KD}}(f(s^{\mathbf{T}}), f(s^{\mathbf{S}})) = \|f(s^{\mathbf{T}}) - f(s^{\mathbf{S}})\|^2 \leq K \cdot c. \quad (5)$$

Proof. The proof is given in the supplementary. \square

The previous theorem indicates that if $c \rightarrow 0$, then the teacher-student reconstruction loss $\mathcal{L}_{\text{rec-KD}}$ is also converging to zero, which confirms our conjecture. In practice, the constant c might not approach zero, *i.e.* it might be hard to optimize $\mathcal{L}_{\text{slot-KD}}$ towards zero. In this case, introducing the teacher-student reconstruction loss into the optimization objective might be useful. We empirically test this objective and find that it does not help convergence to a better optimum. In summary, both theoretical and empirical evidence support our conjecture, suggesting that our simple knowledge distillation objective is sufficient.

4. Experiments

4.1. Datasets

We evaluate SLOTMATCH on both synthetic and real-world video datasets to assess its effectiveness across controlled, real-world and zero-shot scenarios.

MOVi-E. The Multi-Object Video (MOVi-E) dataset [9] is generated using the Kubric simulator, which provides ground-truth object segmentation for precise evaluation. MOVi-E includes up to 23 objects per scene and is filmed

with linear camera motion. The dataset includes complex object interactions, occlusions, and realistic textures. The videos have a 24-frame length and a 256×256 resolution. We use the official train and validation splits.

YTVIS-2021. To evaluate scalability to real-world scenarios, we use the YouTube Video Instance Segmentation 2021 (YTVIS-2021) dataset [33]. It contains unconstrained real-world videos, capturing diverse scenes including indoor/outdoor environments, multiple object categories, and complex interactions. Videos vary in length (up to 76 frames) and resolution. We resize them to 518×518 pixels. We report results on the official split.

DAVIS 2017. We report results on the DAVIS 2017 dataset [27] to evaluate fine-grained segmentation quality. This benchmark provides videos with dense temporal annotations, with every frame labeled using pixel-accurate object masks. The videos span diverse real-world scenarios, including people, animals, vehicles, and sports activities, capturing challenging phenomena like fast motion and cluttered backgrounds.

YTVIS-2021 \rightarrow OVIS. We conduct zero-shot experiments on Occluded Video Instance Segmentation (OVIS) [28], a dataset specifically focused on challenging scenarios. OVIS contains real-world videos with heavy occlusions, making it particularly suitable for testing temporal consistency when objects frequently disappear and reappear. The dataset features 607 training videos and 140 validation videos across 25 object categories.

4.2. Evaluation Metrics

We use two complementary evaluation metrics, namely the Foreground Adjusted Rand Index (FG-ARI) and the mean Best Overlap (mBO), and apply them at both image and video levels. **FG-ARI** measures how well the model groups pixels belonging to the same object. With a range of 0 to 1, and a higher value indicating better performance, its focus is on *object discovery quality*, *i.e.* if the model correctly identifies which pixels belong to the same object. FG-ARI compares predicted object masks against ground-truth segmentation masks. **mBO** measures the spatial precision of object masks, *i.e.* how accurately the predicted masks align with ground-truth boundaries. For each predicted mask, it finds the ground-truth mask with the highest IoU, then averages the IoU across all objects. mBO focuses on *segmentation mask quality*, measuring how precise and well-defined the predicted object boundaries are.

For the image-level evaluation, we compute the FG-ARI and mBO metrics per frame, then average them. For video, we compute the metrics across entire video sequences, accounting for temporal consistency.

4.3. Baselines and Hyperparameters

Baselines. We compare SLOTMATCH against a range of recent object-centric video segmentation models. These in-

Table 1. Comparison of video object segmentation performance on MOVi-E, YTVIS-2021, and DAVIS 2017. We report FG-ARI and mBO scores at both image and video levels. In most cases, SLOTMATCH outperforms both baselines and ablated versions. The top two scores for each metric are highlighted in **blue bold** (top method), **orange bold** (second best).

Method	MOVi-E				YTVIS-2021				DAVIS 2017			
	Image		Video		Image		Video		Image		Video	
	FG-ARI \uparrow	mBO \uparrow										
SAVi [20]	39.2	-	42.8	16.0	-	-	-	-	-	-	-	-
STEVE [31]	54.1	-	50.6	26.6	-	-	15.0	19.1	-	-	-	-
VideoSAUR [34]	78.4	-	73.9	35.6	-	-	28.9	26.3	12.6	23.9	8.3	18.4
VideoSAURv2 [25]	-	-	77.1	34.4	-	-	31.2	29.7	11.8	23.0	7.6	19.2
SOLV [1]	80.8	-	-	-	29.1	-	-	-	32.2	-	-	-
SLOTCONTRAST [25] (teacher)	83.9	32.4	81.7	28.6	45.5	39.7	36.8	32.4	89.1	12.1	73.3	11.8
DINOSAUR [30]	65.1	29.1	-	-	-	-	-	-	-	-	-	-
DIOD [19]	82.2	-	-	-	-	-	-	-	-	-	-	-
Student (no KD)	80.1	28.9	76.6	30.1	44.5	38.8	37.2	32.1	93.7	11.9	76.6	11.6
Feature KD	81.8	31.6	80.1	28.1	45.2	38.2	35.9	31.4	94.6	12.8	91.6	12.7
Reconstruction KD	81.4	31.5	81.1	29.1	44.9	38.8	35.6	31.8	92.0	20.5	88.4	20.3
SLOTMATCH (MSE)	82.1	30.2	78.6	26.4	45.1	39.7	36.9	32.6	94.4	20.0	89.6	20.0
SLOTMATCH + Reconstruction KD	74.4	29.7	66.2	24.1	45.6	38.3	36.1	31.1	96.4	12.7	91.2	12.4
SLOTMATCH (ours)	84.1	33.6	81.8	30.5	45.8	39.8	37.3	32.8	95.6	30.6	92.8	31.6

clude slot-based methods such as SAVi [20], STEVE [31], SOLV [1], VideoSAUR [34], and its DINOv2-enhanced variant, VideoSAURv2 [25]. We reproduce the results of SLOTCONTRAST [25], which serves as the teacher in our framework based on knowledge distillation. We further introduce several new baselines, each employing a different distillation strategy, as follows:

- **DIOD** [19] employs self-distillation to continuously improve motion-guided object discovery via an iterative pseudo-labeling framework.
- **DINOSAUR** [30] trains a student with a particular form of bottleneck that condenses the high-dimensional information from teacher features.
- **Student (no KD)** is a SLOTCONTRAST model trained from scratch, using a smaller encoder version from the same family, namely DINOv2-small instead of DINOv2-base.
- **Feature KD** is a student model (based on DINOv2-small) which distills features from the frozen DINOv2-base teacher encoder. These are passed through a two-layer MLP, and the student is trained to match the transformed features via MSE.
- **Reconstruction KD** distills the reconstructed output of the teacher model to the student model, minimizing the MSE between the two outputs.

We also report results with various ablated versions or alternatives of SLOTMATCH, namely:

- **SLOTMATCH (MSE)** aligns teacher and student slot representations using MSE instead of cosine similarity.
- **SLOTMATCH + Reconstruction KD** combines slot-

level distillation and reconstruction output distillation.

Hyperparameters. We discuss reproducibility details and hyperparameter settings in the supplementary material.

4.4. Results

Quantitative results. In Table 1, we present comparative results on MOVi-E, YTVIS-2021 and DAVIS. Remarkably, SLOTMATCH consistently outperforms all prior methods across these datasets, including its teacher, SLOTCONTRAST [25]. Despite having $3.6\times$ fewer parameters and up to $2.7\times$ faster inference speed than SLOTCONTRAST (as per Table 2), our student achieves higher mask precision (mBO) and comparable or better object separation (FG-ARI). Notably, we improve video mBO on YTVIS from 32.4 (for SLOTCONTRAST) to 32.8 (for SLOTMATCH), while reducing latency by nearly half, showing that accurate object-centric segmentation does not require large models.

We find that mBO improvements are very large on the real-world DAVIS dataset, where the teacher may overfit to slot assignment, but underperform on precise masks. Interestingly, our student avoids this overfitting and better balances separation and alignment. This aligns with our hypothesis that slot supervision can offer better generalization than end-to-end training with larger capacity alone.

Qualitative results. In Figure 3, we present a qualitative comparison of segmentation results produced by the teacher, the student model trained without distillation, and our SLOTMATCH model, across MOVi-E [9] (left-hand side) and YTVIS-2021 [33] (right-hand side).

On MOVi-E, which consists of synthetic scenes with numerous objects, both teacher and student models fail to de-

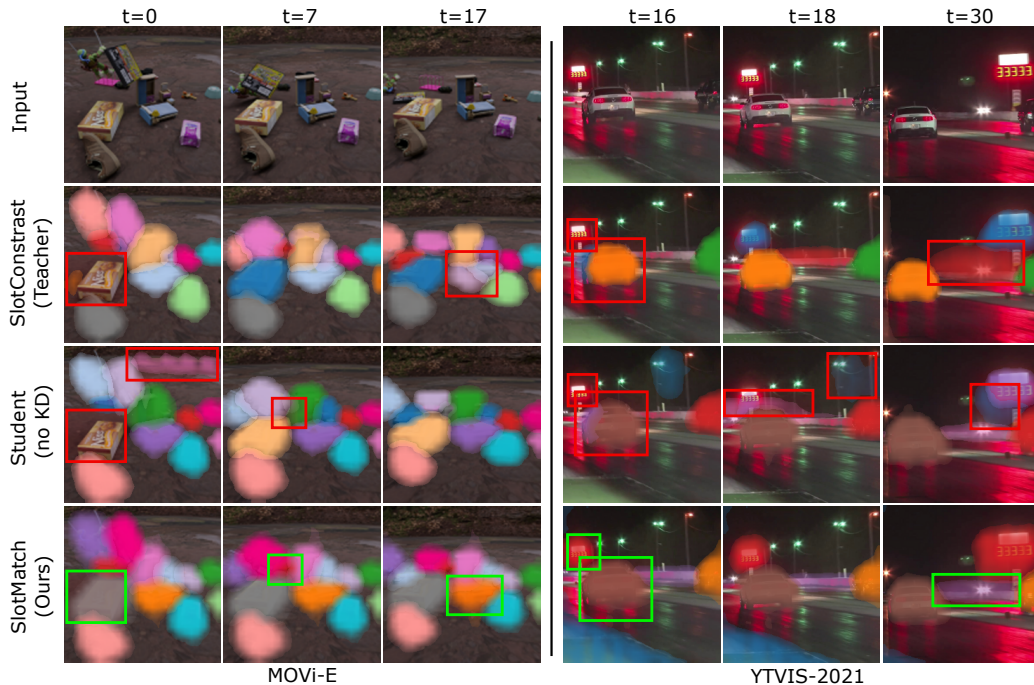


Figure 3. Qualitative segmentation results on MOVi-E (left) and YTVIS-2021 (right). The first row shows raw frames; the second and third rows show slots from the student and teacher models, respectively; the final row presents results from our distillation-based SLOTMATCH. SLOTMATCH recovers missed slots, refines object boundaries, and produces sharper, more consistent slots. Mistakes by the student and teacher models are annotated in red, while corrections and additional detections introduced by SLOTMATCH are highlighted in green. Best viewed in color.

tect certain objects in the initial video frames, *e.g.* the box on the left at $t = 0$. The teacher model suffers from over-clustering (*e.g.* object on the right at $t = 17$), fragmenting single objects into multiple slots, while the student model (without distillation) fails to assign smaller or finer objects to any slot, *e.g.* the one in the center at $t = 7$. In contrast, our student trained with SLOTMATCH consistently recovers missed instances, resolves the over-clustering issue, produces robust slot representations, and maintains temporally consistent slot assignments, *e.g.* consistent coloring of objects from $t = 7$ to $t = 17$.

On YTVIS, a real-world and more challenging dataset with occlusions and poor lighting, we observe similar trends, *i.e.* both teacher and student models exhibit over-clustering in the initial frames, fragmenting single objects into multiple slots. In contrast, SLOTMATCH effectively refines the spatial extent of the masks and mitigates over-segmentation. Furthermore, our method outperforms in both slot assignment (*e.g.* correctly grouping the street light on the left) and boundary delineation (*e.g.* guardrail on the right).

Green boxes indicate new or corrected slots introduced by our method, while red boxes highlight limitations of both the teacher and non-distilled student. These visual improvements confirm that distillation from the slots of a strong teacher not only preserves the original slot grouping, but

Table 2. Comparison of inference speed, number of parameters, and GFLOPs between the SLOTMATCH teacher and our SLOTMATCH student. Measurements are performed on three GPUs (NVIDIA A100 with 40GB VRAM, NVIDIA 3090 with 24GB VRAM, NVIDIA 2080 with 12GB VRAM), using video samples from the YTVIS-2021 dataset.

Method	#Params (M) ↓	#GFLOPs ↓	Inference Time (ms) ↓		
			A100	3090	2080
Teacher	91.0	8825.7	347.4	700.5	916.5
SLOTMATCH	25.2	3266.5	186.0	261.4	331.0
Reduction	3.61×	2.70×	1.87×	2.68×	2.77×

also enhances the student’s robustness to occlusion, lighting variation, and clutter, all in an unsupervised fashion.

Efficiency comparison. In addition to improving segmentation quality, SLOTMATCH significantly reduces computational cost compared to its teacher, SLOTMATCH. As shown in Table 2, our distilled student achieves a reduction of 3.6× in parameters (91M→25M) and 2.7× in FLOPs, respectively. We run our experiments on three GPUs, to assess running time differences in distinct compute environments. We find that our student is between 1.9× and 2.7× faster than its student. The reported gains come with no additional supervision and without sacrificing slot quality or temporal consistency. This highlights the practical benefits of our distillation approach in resource-constrained settings.

Zero-shot generalization. In Table 3, we compare SLO-

Table 3. Zero-shot generalization results on the OVIS dataset, using models trained only on YTVIS (see performance on original dataset in Table 1). We compare the student trained from scratch (no KD) versus our SLOTMATCH student.

Method	Image		Video	
	FG-ARI \uparrow	mBO \uparrow	FG-ARI \uparrow	mBO \uparrow
Student (no KD)	54.6	24.9	34.6	21.5
SLOTMATCH	55.8	25.5	34.8	21.5

Table 4. Ablation study on the YTVIS dataset showing the effect of varying the weight β of the distillation loss $\mathcal{L}_{\text{slot-KD}}$ in SLOTMATCH. The best performance across all metrics is achieved at $\beta = 0.2$.

Method	β	Image		Video	
		FG-ARI \uparrow	mBO \uparrow	FG-ARI \uparrow	mBO \uparrow
Teacher	-	45.5	39.7	36.8	32.4
Student (no KD)	-	44.5	38.8	37.2	32.1
SLOTMATCH	0.1	44.5	39.1	34.9	32.5
	0.2	45.8	39.8	37.3	32.8
	0.3	44.4	39.1	36.3	32.5
	0.5	43.8	38.9	35.5	32.1
	0.8	43.9	38.3	35.4	32.0

MATCH against the student trained from scratch (without distillation), in the zero-shot setup on the challenging OVIS dataset. Notably, SLOTMATCH maintains competitive video-level performance (FG-ARI: 34.8 vs. 34.6) compared with the student trained from scratch, while preserving slightly better spatial mask quality (mBO: 25.5 vs. 24.9). This demonstrates that distilling structured slot representations enhances robustness to occlusion and domain shift.

4.5. Ablation Studies

We conduct ablations to isolate the contribution of each component in our framework. The ablation results are summarized in Tables 1, 4, and 5.

Slot vs. feature and reconstruction KD. To test whether slot representations are the best target for distillation, we compare our method with variants that distill encoder or decoder features via MSE (see Table 1). While feature KD and reconstruction KD bring modest gains over the student (no KD) baseline, they remain below our slot-based formulation, by significant margins. This supports our hypothesis that distilling structured object-centric representations leads to better temporal consistency and segmentation quality.

Cosine vs. MSE loss. We compare the proposed loss based on cosine similarity with an alternative loss based on MSE over slot representations (see Table 1). Cosine-based distillation yields more stable improvements across datasets, especially on YTVIS, likely due to its scale invariance and better alignment with semantic structure in high-dimensional spaces.

With or without reconstruction KD. To empirically determine if the proposed $\mathcal{L}_{\text{slot-KD}}$ loss is sufficient or not, we

Table 5. Comparison of distillation performance with and without Hungarian matching on the MOVIE dataset. Omitting Hungarian matching (as proposed) leads to better performance.

Method	Image		Video	
	FG-ARI \uparrow	mBO \uparrow	FG-ARI \uparrow	mBO \uparrow
SLOTCONTRAST (Teacher)	83.9	32.4	81.7	28.6
Student (no KD)	80.1	28.9	76.6	30.1
SLOTMATCH (w/ matching)	83.5	31.8	81.5	28.6
SLOTMATCH (w/o matching)	84.1	33.6	81.8	30.5

carry out experiments with an enhanced version of SLOTMATCH, where the distillation is also applied over reconstructed features via the $\mathcal{L}_{\text{rec-KD}}$ loss (see Table 1). Perhaps surprisingly, this double distillation procedure degrades performance by considerable margins on MOVIE. The results show that adding additional distillation losses can make the distillation more difficult to tune, eventually leading to inferior results. In summary, the empirical results confirm Theorem 1, indicating that distillation via $\mathcal{L}_{\text{slot-KD}}$ is sufficient.

Distillation weight. We sweep the distillation loss weight β and obtain the best performance at $\beta = 0.2$ (see Table 4). Too little weight underutilizes the teacher signal, while too much harms diversity by forcing alignment too strongly.

Hungarian vs. direct index matching. As slots are inherently permutation-invariant, there is no guarantee for one-to-one alignment between student and teacher slots. This presents a challenge for direct knowledge transfer. To this end, we explore two matching strategies: (i) aligning slots by index positions (proposed option) or (ii) using the Hungarian algorithm to find the most similar slot pairs based on their features, before applying the loss. As shown in Table 5, distillation without Hungarian matching yields better performance in our setup, while also being more computationally efficient. A likely cause for this outcome is that strict matching over-constrains the learning process, negatively impacting the convergence of the distillation model and leading to suboptimal results. Therefore, all results reported in the experiments omit the Hungarian matching step.

5. Conclusion

In this work, we introduced SLOTMATCH, a simple and effective framework for distilling slot-based object representations from a large teacher model into a lightweight student. By aligning slots directly via cosine similarity, our method avoids auxiliary objectives. We showed both theoretically and empirically that this objective is sufficient to transfer semantic structure, leading to a student that outperforms its teacher in segmentation quality, while being significantly more efficient. Our results on MOVIE, YTVIS and DAVIS established new state-of-the-art performance

levels among unsupervised slot-based video models. In future work, we aim to continue our research in scaling down object-centric models for real-world deployment.

References

- [1] Görkay Aydemir, Weidi Xie, and Fatma Guney. Self-supervised object-centric learning for videos. In *Proceedings of NeurIPS*, pages 32879–32899, 2023. 2, 6
- [2] Ondrej Biza, Sjoerd Van Steenkiste, Mehdi SM Sajjadi, Gamaleldin F Elsayed, Aravindh Mahendran, and Thomas Kipf. Invariant slot attention: object discovery with slot-centric reference frames. In *Proceedings of ICML*, pages 2507–2527, 2023. 2
- [3] Christopher Burgess, Loic Matthey, Nicholas Watters, Rishabh Kabra, Irina Higgins, Matt Botvinick, and Alexander Lerchner. MONet: Unsupervised Scene Decomposition and Representation. *arXiv preprint arXiv:1901.11390*, 2019. 1
- [4] Mathilde Caron, Hugo Touvron, Ishan Misra, Hervé Jégou, Julien Mairal, Piotr Bojanowski, and Armand Joulin. Emerging properties in self-supervised vision transformers. In *Proceedings of ICCV*, pages 9650–9660, 2021. 1
- [5] Wojciech Czarnecki, Simon Osindero, Max Jaderberg, Grzegorz Swirszcz, and Razvan Pascanu. Sobolev training for neural networks. In *Proceedings of NeurIPS*, pages 4281–4290, 2017. 2
- [6] Aniket Didolkar, Andrii Zadaianchuk, Rabiul Awal, Maximilian Seitzer, Efstratios Gavves, and Aishwarya Agrawal. CTRL-O: Language-Controllable Object-Centric Visual Representation Learning. In *Proceedings of CVPR*, pages 29523–29533, 2025. 2
- [7] Gamaleldin Elsayed, Aravindh Mahendran, Sjoerd Van Steenkiste, Klaus Greff, Michael Mozer, and Thomas Kipf. SAVi++: Towards end-to-end object-centric learning from real-world videos. In *Proceedings of NeurIPS*, pages 28940–28954, 2022. 2
- [8] Ke Fan, Zechen Bai, Tianjun Xiao, Tong He, Max Horn, Yanwei Fu, Francesco Locatello, and Zheng Zhang. Adaptive slot attention: Object discovery with dynamic slot number. In *Proceedings of CVPR*, pages 23062–23071, 2024. 2
- [9] Saeed Ghorbani, Kimia Mahdavian, Anne Thaler, Konrad Kording, Douglas James Cook, Gunnar Blohm, and Nikolaus Troje. MoVi: A large multi-purpose human motion and video dataset. *PLoS One*, 16(6):e0253157, 2021. 2, 5, 6, 12
- [10] Klaus Greff, Antti Rasmus, Mathias Berglund, Tele Hao, Harri Valpola, and Jürgen Schmidhuber. Tagger: Deep unsupervised perceptual grouping. In *Proceedings of NeurIPS*, 2016. 2
- [11] Klaus Greff, Sjoerd Van Steenkiste, and Jürgen Schmidhuber. Neural expectation maximization. In *Proceedings of NeurIPS*, pages 6694–6704, 2017. 2
- [12] Klaus Greff, Raphaël Lopez Kaufman, Rishabh Kabra, Nick Watters, Christopher Burgess, Daniel Zoran, Loic Matthey, Matthew Botvinick, and Alexander Lerchner. Multi-object representation learning with iterative variational inference. In *Proceedings of ICML*, pages 2424–2433, 2019. 1
- [13] Yuxian Gu, Li Dong, Furu Wei, and Minlie Huang. MiniLLM: Knowledge Distillation of Large Language Models. In *Proceedings of ICLR*, 2024. 2
- [14] Kaiming He, Xinlei Chen, Saining Xie, Yanghao Li, Piotr Dollár, and Ross Girshick. Masked autoencoders are scalable vision learners. In *Proceedings of CVPR*, pages 16000–16009, 2022. 1
- [15] Geoffrey Hinton, Oriol Vinyals, and Jeff Dean. Distilling the knowledge in a neural network. *arXiv preprint arXiv:1503.02531*, 2015. 2
- [16] Adrian Iordache, Bogdan Alexe, and Radu Tudor Ionescu. Multi-level feature distillation of joint teachers trained on distinct image datasets. In *Proceedings of WACV*, pages 7133–7142, 2025. 2
- [17] Baoxiong Jia, Yu Liu, and Siyuan Huang. Improving object-centric learning with query optimization. In *Proceedings of ICLR*, 2023. 2
- [18] Ioannis Kakogeorgiou, Spyros Gidaris, Konstantinos Karantzalos, and Nikos Komodakis. SPOT: Self-Training with Patch-Order Permutation for Object-Centric Learning with Autoregressive Transformers. In *Proceedings of CVPR*, pages 22776–22786, 2024. 2
- [19] Sandra Kara, Hejer Ammar, Julien Denize, Florian Chabot, and Quoc-Cuong Pham. DIOD: Self-Distillation Meets Object Discovery. In *Proceedings of CVPR*, pages 3975–3985, 2024. 2, 6
- [20] Thomas Kipf, Gamaleldin F. Elsayed, Aravindh Mahendran, Austin Stone, Sara Sabour, Georg Heigold, Rico Jonschkowski, Alexey Dosovitskiy, and Klaus Greff. Conditional Object-Centric Learning from Video. In *Proceedings of ICLR*, 2022. 1, 2, 6
- [21] Lei Li, Alexander Linger, Mario Millhaeusler, Vagia Tsiminaki, Yuanyou Li, and Dengxin Dai. Object-centric cross-modal feature distillation for event-based object detection. In *Proceedings of ICRA*, pages 15440–15447, 2024. 2
- [22] Guiqiu Liao, Matjaz Jogan, Eric Eaton, and Daniel A. Hashimoto. FORLA: Federated Object-centric Representation Learning with Slot Attention. In *Proceedings of NeurIPS*, 2025. 2
- [23] Tsung-Yi Lin, Michael Maire, Serge Belongie, James Hays, Pietro Perona, Deva Ramanan, Piotr Dollár, and C Lawrence Zitnick. Microsoft COCO: Common Objects in Context. In *Proceedings of ECCV*, pages 740–755, 2014. 11
- [24] Francesco Locatello, Dirk Weissenborn, Thomas Unterthiner, Aravindh Mahendran, Georg Heigold, Jakob Uszkoreit, Alexey Dosovitskiy, and Thomas Kipf. Object-centric learning with slot attention. In *Proceedings of NeurIPS*, pages 11525–11538, 2020. 1, 2
- [25] Anna Manasyan, Maximilian Seitzer, Filip Radovic, Georg Martius, and Andrii Zadaianchuk. Temporally consistent object-centric learning by contrasting slots. In *Proceedings of CVPR*, pages 5401–5411, 2025. 2, 3, 4, 6, 11
- [26] Maxime Oquab, Timothée Darcet, Théo Moutakanni, Huy Vo, Marc Szafraniec, Vasil Khalidov, Pierre Fernandez, Daniel Haziza, Francisco Massa, Alaaeldin El-Nouby, et al. DINOv2: Learning robust visual features without supervision. *Transactions on Machine Learning Research*, 2024. 1, 2, 3

- [27] F. Perazzi, J. Pont-Tuset, B. McWilliams, L. Van Gool, M. Gross, and A. Sorkine-Hornung. A benchmark dataset and evaluation methodology for video object segmentation. In *Proceedings of CVPR*, pages 724–732, 2016. 2, 5, 11, 12
- [28] Jiyang Qi, Yan Gao, Yao Hu, Xinggang Wang, Xiaoyu Liu, Xiang Bai, Serge Belongie, Alan Yuille, Philip H.S. Torr, and Song Bai. Occluded Video Instance Segmentation: A benchmark. *International Journal of Computer Vision*, 130(8):2022–2039, 2022. 5, 12
- [29] Adriana Romero, Nicolas Ballas, Samira Ebrahimi Kahou, Antoine Chassang, Carlo Gatta, and Yoshua Bengio. FitNets: Hints for Thin Deep Nets. *arXiv preprint arXiv:1412.6550*, 2014. 2
- [30] Maximilian Seitzer, Max Horn, Andrii Zadaianchuk, Dominik Zietlow, Tianjun Xiao, Carl-Johann Simon-Gabriel, Tong He, Zheng Zhang, Bernhard Schölkopf, Thomas Brox, et al. Bridging the gap to real-world object-centric learning. In *Proceedings of ICLR, 2023*. 2, 6, 11
- [31] Gautam Singh, Yi-Fu Wu, and Sungjin Ahn. Simple unsupervised object-centric learning for complex and naturalistic videos. In *Proceedings of NeurIPS*, pages 18181–18196, 2022. 2, 6
- [32] Charig Yang, Hala Lamdouar, Erika Lu, Andrew Zisserman, and Weidi Xie. Self-supervised video object segmentation by motion grouping. In *Proceedings of ICCV*, pages 7177–7188, 2021. 2
- [33] Linjie Yang, Yuchen Fan, Yang Fu, and Ning Xu. The 3rd large-scale video object segmentation challenge - video instance segmentation track, 2021. 2, 5, 6, 12
- [34] Andrii Zadaianchuk, Maximilian Seitzer, and Georg Martius. Object-centric learning for real-world videos by predicting temporal feature similarities. In *Proceedings of NeurIPS*, pages 61514–61545, 2023. 2, 6, 11

In the supplementary, we include the demonstration for Theorem 1, additional quantitative and qualitative results, as well as reproducibility details.

A. Theoretical Demonstration

We next provide the proof of our theorem.

Proof. The cosine similarity between two (teacher and student) slots is defined as:

$$\cos \theta = \frac{\langle s^{\mathbf{T}}, s^{\mathbf{S}} \rangle}{\|s^{\mathbf{T}}\| \cdot \|s^{\mathbf{S}}\|}. \quad (6)$$

By replacing the definition from Eq. (6) in Eq. (4), we obtain the following:

$$\mathcal{L}_{\text{slot-KD}}(s^{\mathbf{T}}, s^{\mathbf{S}}) = 1 - \cos \theta = c, \quad (7)$$

which implies that:

$$\cos \theta = 1 - c. \quad (8)$$

We next express the sum of squared errors (squared Euclidean distance) between slots $\|s^{\mathbf{T}} - s^{\mathbf{S}}\|^2$ in terms of θ .

We start from the following definition:

$$\|s^{\mathbf{T}} - s^{\mathbf{S}}\|^2 = \|s^{\mathbf{T}}\|^2 + \|s^{\mathbf{S}}\|^2 - 2 \cdot \langle s^{\mathbf{T}}, s^{\mathbf{S}} \rangle. \quad (9)$$

From Eq. (6), the scalar product between slots can be written as follows:

$$\langle s^{\mathbf{T}}, s^{\mathbf{S}} \rangle = \|s^{\mathbf{T}}\| \cdot \|s^{\mathbf{S}}\| \cdot \cos \theta. \quad (10)$$

Hence, Eq. (9) becomes:

$$\|s^{\mathbf{T}} - s^{\mathbf{S}}\|^2 = \|s^{\mathbf{T}}\|^2 + \|s^{\mathbf{S}}\|^2 - 2 \cdot \|s^{\mathbf{T}}\| \cdot \|s^{\mathbf{S}}\| \cdot \cos \theta. \quad (11)$$

By employing the following the assumption, specified in Theorem 1:

$$\|s^{\mathbf{T}}\| = \|s^{\mathbf{S}}\| = r, \quad (12)$$

we obtain:

$$\begin{aligned} \|s^{\mathbf{T}} - s^{\mathbf{S}}\|^2 &= 2 \cdot r^2 - 2 \cdot r^2 \cos \theta \\ &= 2 \cdot r^2 \cdot (1 - \cos \theta). \end{aligned} \quad (13)$$

By substituting Eq. (8) in Eq. (13), we obtain the following:

$$\|s^{\mathbf{T}} - s^{\mathbf{S}}\|^2 = 2 \cdot r^2 \cdot c. \quad (14)$$

The Lipschitz property of f gives us the following inequality:

$$\|f(s^{\mathbf{T}}) - f(s^{\mathbf{S}})\| \leq K_f \cdot \|s^{\mathbf{T}} - s^{\mathbf{S}}\|. \quad (15)$$

Squaring both sides leads to:

$$\|f(s^{\mathbf{T}}) - f(s^{\mathbf{S}})\|^2 \leq K_f^2 \cdot \|s^{\mathbf{T}} - s^{\mathbf{S}}\|^2. \quad (16)$$

Note that the left term in Eq. (16) is equal to $\mathcal{L}_{\text{rec-KD}}$, i.e.:

$$\mathcal{L}_{\text{rec-KD}}(f(s^{\mathbf{T}}), f(s^{\mathbf{S}})) \leq K_f^2 \cdot \|s^{\mathbf{T}} - s^{\mathbf{S}}\|^2 \quad (17)$$

We next substitute Eq. (14) inside Eq. (17) and obtain:

$$\mathcal{L}_{\text{rec-KD}}(f(s^{\mathbf{T}}), f(s^{\mathbf{S}})) \leq 2 \cdot K_f^2 \cdot r^2 \cdot c. \quad (18)$$

Let $K = 2 \cdot K_f^2 \cdot r^2$. Finally, we obtain:

$$\mathcal{L}_{\text{rec-KD}}(f(s^{\mathbf{T}}), f(s^{\mathbf{S}})) \leq K \cdot c, \quad (19)$$

which concludes the proof of Theorem 1. \square

Remarks:

- If the slots are normalized (i.e. $r = 1$), the bound simplifies to:

$$\mathcal{L}_{\text{rec-KD}}(f(s^{\mathbf{T}}), f(s^{\mathbf{S}})) \leq 2 \cdot K_f^2 \cdot c. \quad (20)$$

- In neural networks, the constant K_f depends on the weights and activations of the model, and it can be estimated via spectral norms.

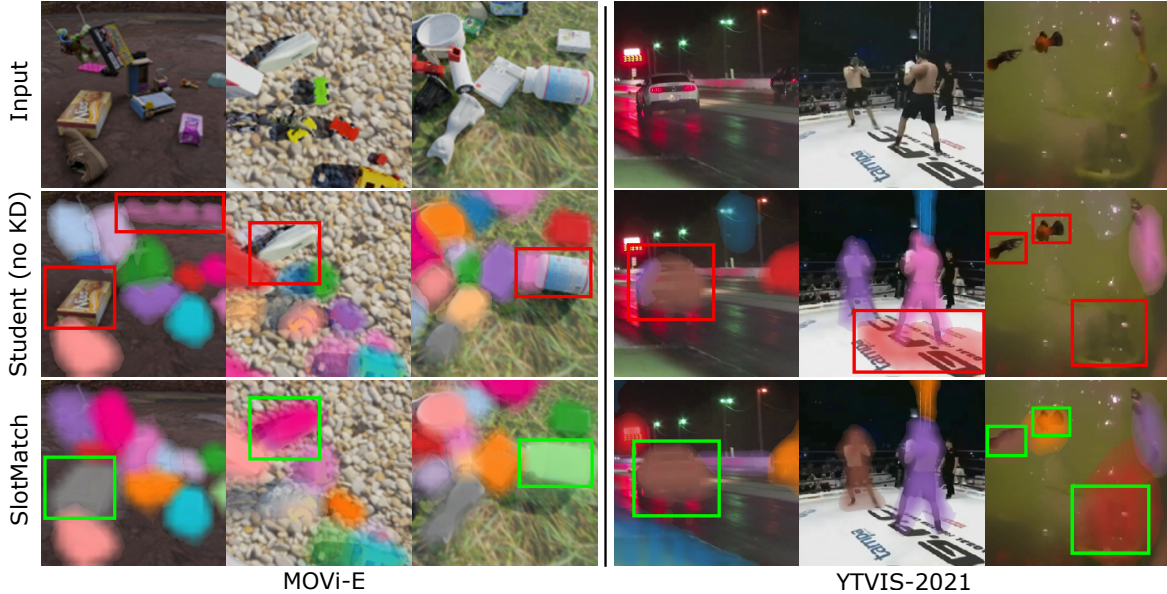


Figure 4. Qualitative comparison on MOVi-E (left) and YTVIS-2021 (right). The second row shows outputs from the student model, while the third row presents results from our distillation-based SLOTMATCH. Student errors, including missed slots, are marked in red. Corrections and additional slots introduced by SLOTMATCH are highlighted in green. Best viewed in color.

Table 6. Video segmentation results on DAVIS [27] with two different teacher models, VideoSAUR [34] and VideoSAURv2 [25]. The top two scores for each metric are highlighted in blue bold (top method), orange bold (second best).

Method	Image mBO \uparrow	Video mBO \uparrow
VideoSAUR [34] (teacher)	23.9	18.4
Student (no KD)	17.4	14.4
SLOTMATCH (ours)	30.3	23.2
VideoSAURv2 [25] (teacher)	23.0	19.2
Student (no KD)	22.9	18.2
SLOTMATCH (ours)	31.2	28.9

B. Additional Results

Qualitative results. In Figure 4, we showcase qualitative comparisons of segmentation masks on challenging examples from MOVi-E and YTVIS. Our method produces sharper and more temporally-consistent masks than the student model without distillation. On MOVi-E, SLOTMATCH segments overlapping or partially occluded objects more cleanly, while on real-world YTVIS data, it shows improved boundary alignment and fewer slot collisions. These results highlight the benefit of slot-level supervision in guiding the student towards focusing on meaningful object structure.

Results with different teachers. In Table 6, we report results with additional teacher models, namely VideoSAUR [34] and VideoSAURv2 [25], on the DAVIS [27] dataset. The SLOTMATCH student based on DINOv2 is compared with an equivalent architecture without distillation (no KD), as well as its corresponding teacher model. The results fol-

Table 7. Image segmentation results on MS COCO [23] with DINO SAURv2 [30] as teacher. The top two scores for each metric are highlighted in blue bold (top method), orange bold (second best).

Method	Image FG-ARI \uparrow	Image mBO \uparrow
DINO SAURv2 [30] (teacher)	44.7	29.3
Student (no KD)	41.5	28.6
SLOTMATCH (ours)	42.3	28.8

low the same trend as in the main experiments, *i.e.* SLOTMATCH consistently outperforms both the student (no KD) and teacher models. These results confirm that SLOTMATCH generalizes across multiple teacher models.

Image segmentation results. In Table 7, we present image segmentation results on the MS COCO [23] dataset, employing DINO SAURv2 [30] as teacher. SLOTMATCH surpasses the analogous model (without distillation), but remains below the teacher. We conclude that SLOTMATCH can obtain competitive results in image segmentation, with a reduced computational cost. Yet, the true benefit of SLOTMATCH is more obvious in video segmentation, where its ability to maintain temporal consistency of slots plays a key role.

C. Reproducibility Details

Model configurations. In Table 8, we provide a complete overview of model and training hyperparameters used across all experiments. The teacher and student models share a common slot attention architecture, decoder, and

Table 8. Summary of key hyperparameters for all teacher and student models used in our experiments. All models use the same decoder, predictor, and loss weights.

Hyperparameter	MOVi-E		YTVIS-2021		DAVIS 20217	
	Teacher	Student	Teacher	Student	Teacher	Student
Backbone	ViT-B/14	ViT-S/14	ViT-B/14	ViT-S/14	ViT-B/14	ViT-S/14
Feature size (m)	768	384	768	384	768	384
Slot dim (S)	128	128	64	64	128	128
#Slots (N)	15	15	7	7	4	4
Input size	336×336	336×336	518×518	518×518	336×336	336×336
#Patches	576	576	1369	1369	576	576
Batch size (B)	16	16	64	64	16	16
Learning rate (η)	0.0004	0.0004	0.0008	0.0008	0.0008	0.0008
Total steps	300K	300K	100K	100K	100K	100K
Loss weights (α, β)	(1, 0.2)					
Slot attention iterations	2					
Contrastive temperature (τ)	0.1					
Gradient clip	0.05					
Predictor	Transformer (1×4)					

Table 9. Approximate training time per experiment on two A100 GPUs.

Method	Dataset	Steps	GPU Hours
SLOTMATCH	MOVi-E	300K	≈ 138
	YTVIS	100K	≈ 39
	DAVIS	100K	≈ 25

Table 10. Robustness evaluation of SLOTMATCH on the YTVIS dataset using three random seeds (42, 101, 2048). The last row reports the average performance across seeds. Consistent results across runs indicate stable training.

Run	Seed	Video FG-ARI ↑	Video mBO ↑
Run 1	42	37.2	33.1
Run 2	101	37.4	32.4
Run 3	2048	37.3	32.9
Mean	-	37.3	32.8
Std.	-	±0.06	±0.29

loss structure. For both datasets, the student differs by using a ViT-S/14 encoder with lower feature dimensionality. Other parameters such as slot count, learning rate, and contrastive loss temperature are held constant. These settings enable consistent and reproducible evaluation of our SLOTMATCH distillation approach.

Training time and compute resources. All experiments were conducted using two NVIDIA A100 GPUs (each with 40GB of VRAM). Training the student model on MOVi-E for 300K steps took approximately 138 hours. For YTVIS-2021, training required about 39 hours for 100K steps. All models were implemented in PyTorch Lightning. Total GPU hours for each experiment are summarized in Table 9.

Random seeds and repeated runs. To evaluate the robustness of our method, all reported results are averaged

across three runs using the following seeds: 42, 101 and 2048. Reported results in Table 10 reflect the average performance across these runs. In preliminary experiments, we found the standard deviation for FG-ARI, and mBO across seeds to be within ± 0.06 and ± 0.29 on YTVIS, indicating stable convergence behavior. All random seeds were set using PyTorch Lightning’s `seed_everything` function, as well as each independent module’s respective seed function, to ensure full reproducibility.

Data access and preprocessing. We used public benchmark datasets: MOVi-E [9], YTVIS-2021 [33], DAVIS [27] and OVIS [28]. All datasets are publicly available and can be downloaded from the respective official repositories. Preprocessing for MOVi-E follows the original 336×336 center crop and normalization to $[-1, 1]$. For YTVIS, frames are resized using short-side resizing to 518 pixels with central cropping. OVIS is used for evaluation only. Temporal chunks of 4 frames are sampled per video for both training and evaluation. The corresponding preprocessing and data-related details are present in the configuration files.

Pretrained models and licensing. We will release pre-trained weights for both teacher and student models on all datasets in our code repository. Checkpoints will be provided with instructions for loading and evaluation. The code is released under the CC-BY-NC 4.0 license, and all dependencies are listed in the `environment.yml` file. The repository includes inference scripts, training pipelines, and evaluation tools for FG-ARI and mBO, along with an example configuration to reproduce results.